Supporting Information:

Hierarchical On-Surface Synthesis of Graphene Nanoribbon Heterojunctions

Christopher Bronner[‡,1,], Rebecca A. Durr[‡,2], Daniel J. Rizzo[1], Yea-Lee Lee[1,3], Tomas Marangoni[2], Alin Miksi Kalayjian[2], Henry Rodriguez[1], William Zhao[1], Steven G. Louie[1,4], Felix R. Fischer[2,4,5,]*, Michael F. Crommie[1,4,5,]**

[1]Department of Physics, University of California, Berkeley, CA 94720, USA. [2]Department of Chemistry, University of California, Berkeley, CA 94720, USA. [3]Department of Physics, Pohang University of Science and Technology, Pohang, Kyungbuk, 37673, Korea. [4]Materials Sciences Division, Lawrence Berkeley National Laboratory, Berkeley, CA 94720, USA. [5]Kavli Energy NanoSciences Institute at the University of California Berkeley and the Lawrence Berkeley National Laboratory, Berkeley, California 94720, USA.

* Corresponding authors

‡ These authors contributed equally to this work

1. Control Experiments Demonstrating the Effect of Hierarchical Growth

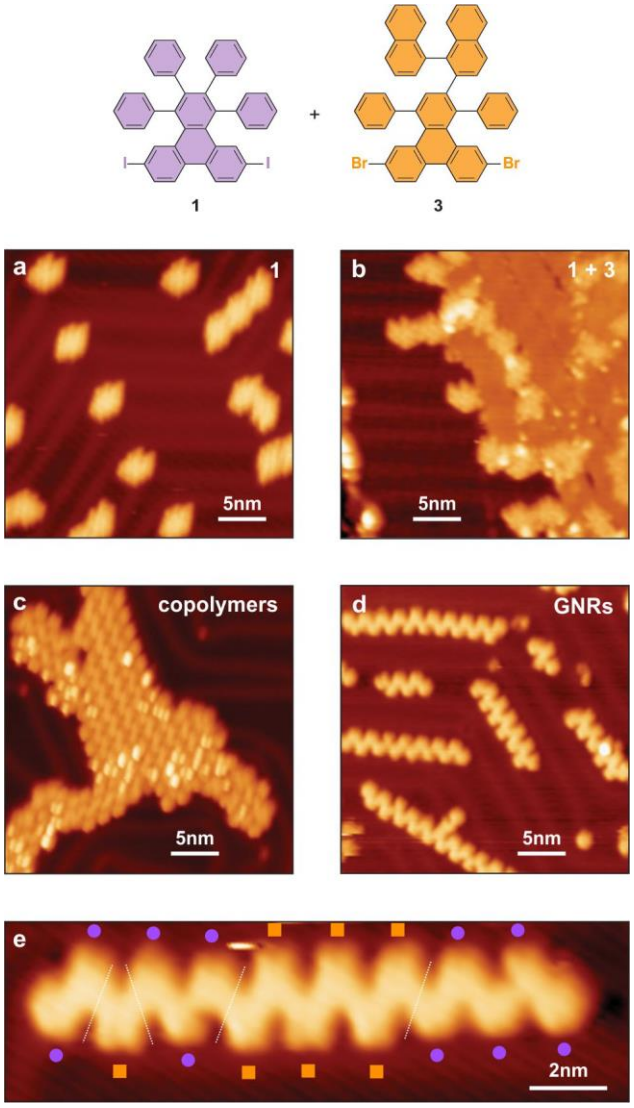

Supporting Figure S1. Control experiment omitting the linker molecule. (a) STM image of **1** on Au(111) (V = 1.0 V, I = 20 pA). (b) STM image of **1** and **3** co-adsorbed on Au(111) (V = 2.0 V, I = 20 pA). (c) Copolymer island after annealing to 230 °C (V = 1.0 V, I = 20 pA). (d) GNRs observed after annealing to 320 °C (V = 0.3 V, I = 40 pA). (e) Magnified GNR exhibiting four heterojunctions (V = 0.3 V, I = 40 pA). Purple round markers indicate cGNR segments, orange square markers indicate binaph-cGNR segments.

As described in the main text, two control experiments were conducted to assess the impact of the hierarchical growth strategy on the control of the copolymer growth sequence. The first control experiment is shown in Supporting Fig. S1. Monomers **1** and **3** were deposited onto a clean Au(111) surface (Supporting Figs. S1a,b) and annealed at 230 °C resulting in islands of

copolymers in which binaphthyl segments are evident as taller protrusions (Supporting Fig. 1c). Further annealing at 320 °C induced cyclodehydrogenation (Supporting Figs. 1d,e). Fig. 4c in the main article shows that compared to the full hierarchical protocol using precursors **1**–**3**, significantly fewer GNRs possess only a single heterojunction, indicating that the linker molecule **2** (omitted in this first control experiment) increases the degree of control over the growth sequence.

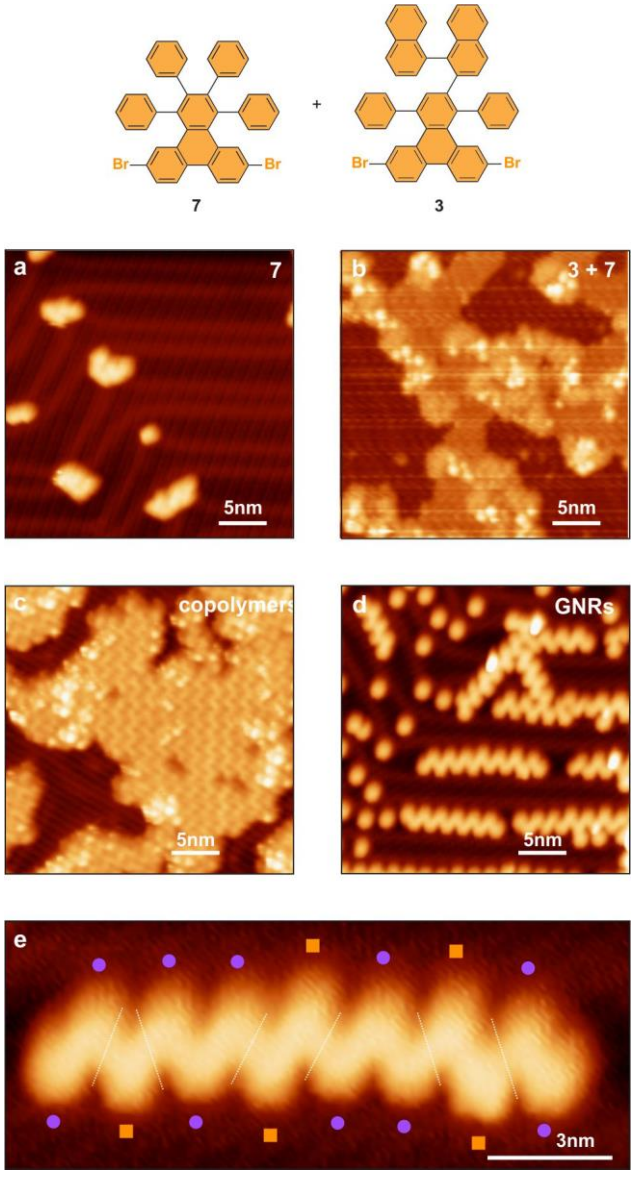

Supporting Figure S2. Control experiment using only brominated precursors. (a) STM image of **7** deposited on Au(111) (V = 1.0 V, I = 30 pA). (b) STM image of **7** and **3** co-deposited on Au(111) (V = 1.0 V, I = 20 pA). (c) Copolymer island after annealing to 190 °C (V = 1.0 V, I = 20 pA). (d) STM image of GNRs obtained after annealing to 330 °C (V = 0.3 V, I = 40 pA).

(e) Magnified image of GNR with six heterojunctions (V = 0.3 V, I = 40 pA). Purple round markers indicate cGNR segments, orange square markers indicate binaph-cGNR segments.

The second control experiment shown in Supporting Fig. S2 uses only brominated precursors, namely **7** and **3**. After sequential deposition (Supporting Figs. S2a,b) of the monomers on Au(111), they were annealed at 190 °C resulting in islands of copolymers (Supporting Fig. S2c). Further annealing at 330 °C leads to cyclodehydrogenation and yields GNRs (Supporting Figs. S2d,e). Fig. 4c in the main article shows that using precursors **7** and **3**, there is a higher relative occurrence of GNRs with more than four heterojunctions and a dramatically reduced occurrence of single-junction GNRs compared to both the preparation using **1** and **3** (partial hierarchical protocol) and the full hierarchical protocol using **1**–**3**.

The comparison between the two control experiments demonstrates that substituting one of the monomers with iodine significantly increases the control over the growth sequence as indicated by the number of heterojunctions in a given GNR. The two control experiments combined demonstrate that the hierarchical growth strategy as implemented in the full hierarchical protocol using **1**–**3** results in an increase of control in GNR heterojunction synthesis.

2. Length Distribution of GNRs

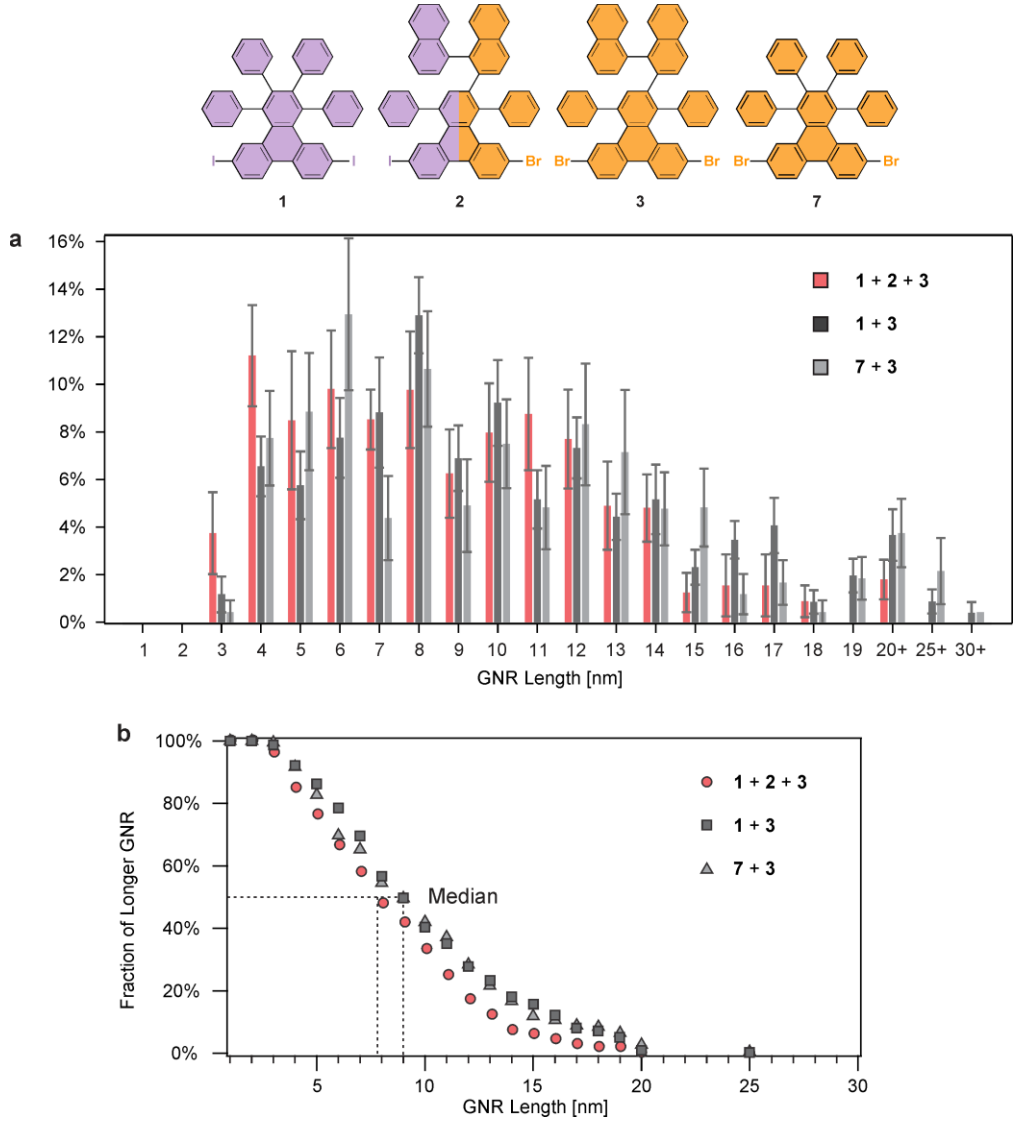

Supporting Figure S3. Length distribution of GNRs. (a) Length histograms for the three different heterojunction preparations on Au(111) using the three different growth protocols. (b) Integrated histogram for the three different growth protocols showing the fraction of GNRs longer than a given length. The median GNR length can be read as indicated.

Supporting Fig. S3a shows the length distribution of the GNR heterostructures that were obtained in the three different growth protocols using different combinations of precursors, namely using precursors **1**–**3** (full hierarchical protocol), **1** and **3** (partial hierarchical protocol) and **7** and **3** (random protocol). No significant differences in the length distribution can be observed for the three cases. The majority of GNRs possesses a length between 4 and 20 nm. In Supporting Fig. S3b, the histograms were integrated to show the fraction of GNRs which exceed a given length.

From this diagram, the median length can be directly obtained. In all three cases the median length is 8 or 9 nm.

3. Original STM image of GNR Heterostructures

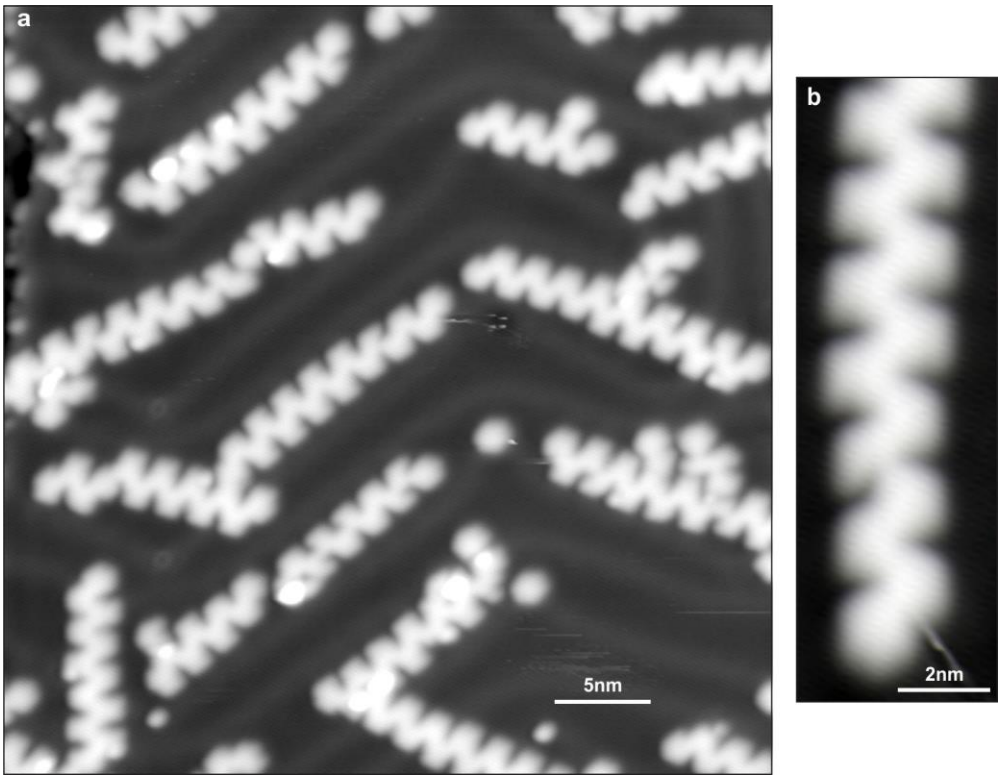

Supporting Figure S4. Original STM images of GNR heterostructures. (a) STM image of GNR heterostructures shown in Fig. 4a without overlaid tinting (V = 0.3 V, I = 20 pA). (b) STM image of the GNR heterostructure shown in Fig. 4b without overlaid tinting (V = 0.3 V, I = 20 pA).

The STM images of GNR heterostructures in the main article were tinted to help identify cGNR and binaph-cGNR segments. Supporting Fig. S4 shows the original, unprocessed images that were used in Figs. 4a,b.

4. Calculated Projected Density of States (PDOS) of GNR Heterojunction

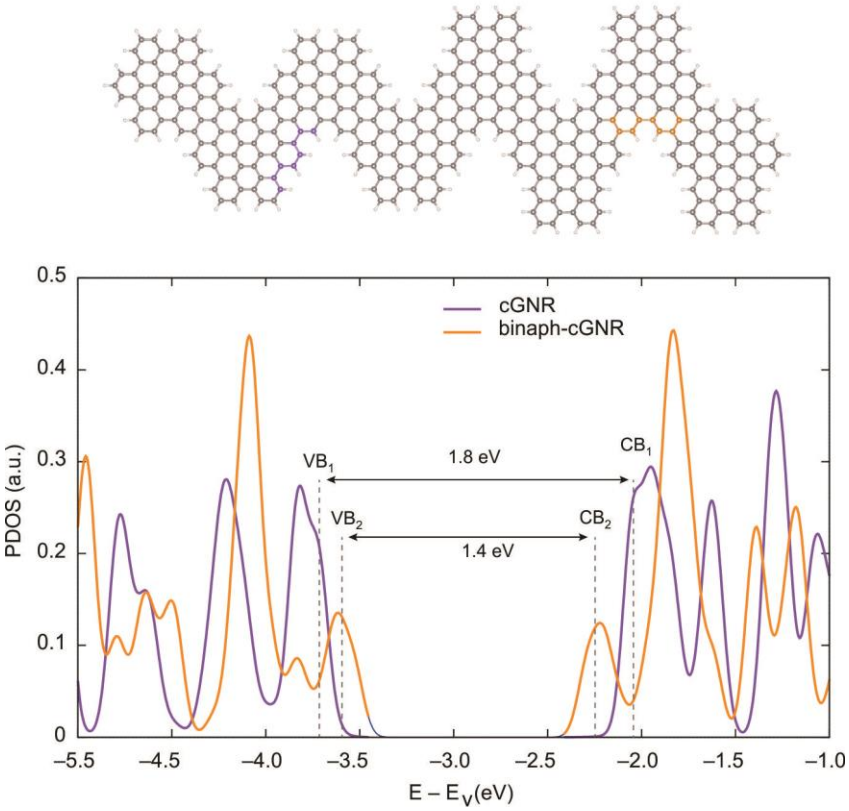

Supporting Figure S5. Electronic structure of cGNR and binaph-cGNR segments from DFT calculations. PDOS averaged in the cGNR (purple) and binaph-cGNR (orange) segment of a single molecular GNR heterojunction. The horizontal axis denotes the energy relative to the vacuum level. The band gap energies of cGNR and binaph-cGNR are given by 1.8 eV and 1.4 eV, respectively.

We have calculated the projected density of states (PDOS) using the Kohn-Sham states within LDA-DFT for a cGNR/binaph-cGNR heterojunction (the unit cell is shown in Supporting Fig. S5) in order to compare with the differential conductance spectra in Fig. 5 of the main text. To mimic the broadening of the STM tip, the PDOS is obtained over an average of eight carbon atoms in each area (as highlighted in purple and orange for cGNR and binaph-cGNR, respectively (Supporting Fig. S5, top)). The simulated PDOS spectral density (Supporting Fig. S5) is qualitatively similar to the experimental STS results (including a particularly large PDOS intensity for the CB+1 band in the binaphthyl segment). In the LDA-DFT calculations the gap energies of the cGNR and binaph-cGNR segments in the heterojunction are given by 1.8 eV and 1.4 eV. If we include electron correlation effects to the self energy of the electron states within the GW

approximation, the band gap increases to the large values (3.63 eV for a cGNR). Furthermore, if we included the screening from the gold substrate, the band gap energy would be reduced again similar to the former study on 7-13 AGNR heterojunctions.[1] These two effects account for the difference of the band gap magnitude between the LDA calculations and the STS experiments.

5. Synthesis of Molecular Precursors

Materials and General Methods. Unless otherwise stated, all manipulations of air and/or moisture sensitive compounds were carried out in oven-dried glassware, under an atmosphere of N_2. All solvents and reagents were purchased from Alfa Aesar, Spectrum Chemicals, Acros Organics, TCI America, and Sigma-Aldrich and were used as received unless otherwise noted. Organic solvents were dried by passing through a column of alumina and were degassed by vigorous bubbling of N_2 through the solvent for 20 min. Flash column chromatography was performed on SiliCycle silica gel (particle size 40–63 μm). Thin layer chromatography was carried out using SiliCycle silica gel 60 Å F-254 precoated plates (0.25 mm thick) and visualized by UV absorption. All ^{1}H and {^{1}H}^{13}C NMR spectra were recorded on Bruker AV-600, AV-500, and AVQ-400 spectrometers, and are referenced to residual solvent peaks ($C_2D_2Cl_4$ ^{1}H NMR δ = 6.0 ppm, ^{13}C NMR δ = 73.8 ppm; $CDCl_3$ ^{1}H NMR δ = 7.26 ppm, ^{13}C NMR δ = 77.2 ppm; $(CD_3)_2SO$ ^{1}H NMR δ = 2.50, ^{13}C NMR δ = 39.5); ESI-HRMS mass spectrometry was performed on a Finnigan LTQ FT (Thermo) *via* direct injection using a flow rate of 5.0 μL min^{-1}. X-ray quality single crystals of **2** were obtained by recrystallization from a MeOH/$CHCl_3$ solution. X-ray crystallography of **2** was performed on an APEX II QUAZAR, using a Microfocus Sealed Source (Incoatec; Cu-Kα radiation), Kappa Geometry with DX (Bruker-AXS build) goniostat, a Bruker APEX II detector, QUAZAR multilayer mirrors as the radiation monochromator, and Oxford Cryostream 700 held at 100 K. Crystallographic data were resolved with SHELXT, refined with SHELXL-2014, and visualized with ORTEP-32. Compounds 6,11-diiodo-1,2,3,4-tetraphenyltriphenylene (**1**), 6,11-dibromo-1,2,3,4-tetraphenyltriphenylene (**7**), and 2,7-dibromophenanthrene-9,10-dione were synthesized following previously reported literature procedures.[2,3]

2-Bromo-1,1'-binaphthyl (8): A 50 mL 2-neck round bottom flask was charged with 2,2'-dibromo-1,1'-dinaphthyl (0.98 g, 2.4 mmol) and dry THF (15 mL). The solution was cooled to −40 °C, ^{n}BuLi (2.5 M in hexanes, 2.4 mmol) was added dropwise and the reaction mixture was stirred for 1 h at −40 °C. The reaction mixture was cooled to −78 °C, HCl (1 N, 11.8 mmol) added dropwise, and the reaction mixture was warmed to 25 °C. The solution was concentrated on a rotary evaporator. The residue was dissolved in Et_2O (50 mL) and hydrolyzed with 1 N HCl (50 mL). The reaction mixture was extracted with Et_2O, the combined organic layers were washed

with saturated aqueous $NaHCO_3$ solution, water, and saturated aqueous NaCl solution, and dried over $MgSO_4$. The reaction mixture was concentrated on a rotary evaporator to give **8** (0.72 g, 92%) as a colorless solid. Spectroscopic data is consistent with literature reports.[4] ^{1}H NMR (400 MHz, 25 °C, $CDCl_3$) δ = 8.09 (dd, J = 13.4, 8.3 Hz, 2 H), 7.99 (d, J = 8.2 Hz, 1H), 7.96−7.87 (m, 2H), 7.74 (t, J = 8.1 Hz, 1H), 7.65−7.48 (m, 3H), 7.46−7.38 (m, 2H), 7.38−7.28 (m, 2H) ppm.

2-ethynyl-1,1'-binaphthalene (9): A 25 mL sealable Schlenk flask was charged with **8** (305 mg, 0.75 mmol) in diisopropyl amine (11 mL) and THF (3 mL). $Pd(PPh_3)_4$ (106 mg, 0.08 mmol) and CuI (10 mg, 0.04 mmol) were added, and the reaction mixture was degassed. TMSA (2 mL) was added, and the flask was sealed and stirred at 55 °C for 20 h. The reaction mixture was cooled to 25 °C, and extracted with Et_2O. The combined organic layers were dried over $MgSO_4$, and concentrated on a rotary evaporator. Column chromatography (hexanes) yielded an inseparable mixture of partially deprotected **9**. The intermediate was redissolved in THF (8 mL) and MeOH (8 mL). K_2CO_3 (1 g) was added, and the reaction mixture was stirred at 25 °C for 2 h. The reaction mixture was extracted with CH_2Cl_2, and the combined organic layers were washed with H_2O, dried over $MgSO_4$, and concentrated on a rotatory evaporator. Column chromatography (hexane/CH_2Cl_2 1:0–10:1) yielded **9** (170 mg, 81%) as a colorless oil. Spectroscopic data is consistent with literature reports.[5] ^{1}H NMR (400 MHz, 25 °C, $CDCl_3$) δ = 8.03–7.86 (m, 4H), 7.71 (d, J = 8.6 Hz, 1H), 7.65–7.58 (m, 1H), 7.53–7.43 (m, 3H), 7.33–7.17 (m, 4H), 2.8 (s, 1H) ppm.

2-([1,1'-binaphthalen]-2-yl)-6,11-dibromo-1,4-diphenyltriphenylene (3): A 2-neck 50 mL round bottom flask was charged with 2,7-dibromophenanthrene-9,10-dione (1.0 g, 2.7 mmol) in MeOH (5.7 mL). Diphenyl acetone (5.1 g, 3.6 mmol) was added and the reaction mixture was heated to 75 °C. KOH (0.16 g, 2.9 mmol) in MeOH (9.8 mL) was added drop-wise, and the reaction mixture was heated at 75 °C for 2 h. The reaction was cooled to 25 °C, and filtered. The precipitate was washed with EtOH to yield the intermediate cyclopentadienone as a green solid, which was used without further purification. A 10 mL Schlenk flask was charged with the crude cyclopentadienone (19 mg, 0.036 mmol) and **9** (11 mg, 0.039 mmol) in Ph_2O (0.7 mL), and the reaction mixture was heated to 145 °C for 16 h. The reaction mixture was cooled to 25 °C, and the solvent was evaporated to yield a crude residue. Column chromatography (CH_2Cl_2/hexane 1:10) yielded **3** (21 mg, 76%) as a colorless solid. Variable temperature NMR in 1,1,2,2-tetrachloroethane-d_2 at 110 °C was performed in order to resolve NMR spectroscopic signals (Supporting Fig. S6). Even at high temperature, a fully resolved NMR was not obtained due to the

high barrier to rotation within the molecule. Major NMR shifts at 22 °C reported as follows (Supporting Figs. S8, S9). ^{1}H NMR (600 MHz, $CDCl_3$) δ = 8.13 (d, J = 8.7 Hz, 1H), 7.93 (m, 1H), 7.91 (m, 1H), 7.70–7.64 (m, 2H), 7.47–7.38 (m, 4H), 7.26–7.09 (m, 3H), 6.73 (s, 1H) ppm; ^{13}C NMR (151 MHz, $CDCl_3$) δ = 143.5, 141.6, 138.6, 137.7, 137.2, 133.7, 133.5, 132.8, 131.7, 130.2, 129.9, 129.7, 129.6, 129.2, 128.0, 127.6, 127.6, 127.2, 127.0 (2C), 126.6, 126.2 (2C), 126.1, 125.7, 125.4, 124.7, 124.6 120.1 ppm. HRMS (EI) m/z: $[C_{50}H_{30}Br_2]^+$, calcd. for $[C_{50}H_{30}Br_2]$ 790.0681; found 790.0694.

2-iodophenanthrene-9,10-dione (10): A 5 mL sealable flask was charged with 9,10-phenanthrene quinone (0.25 g, 1.2 mmol) and cooled to 0 °C. Trifluoromethanesulfonic acid (1.0 mL) was added, and the reaction mixtures was stirred under N_2 for 10 min. *N*-Iodosuccinimide (0.54 g, 2.4 mmol) was added slowly to the suspension. The reaction was poured onto ice (100 mL) and the precipitate was filtered to yield **10** (0.07 g, 18%) as an orange solid. Spectroscopic data is consistent with literature reports.[6] ^{1}H NMR (400 MHz, 25 °C, DMSO-d_6) δ = 8.36–8.20 (m, 2H), 8.10–8.03 (m, 3H), 7.78 (t, J = 7.7 Hz, 1H), 7.56 (t, 7.5 Hz, 1H) ppm; HRMS (EI) m/z: $[C_{14}H_7O_2I]^+$, calcd. for $[C_{14}H_7O_2I]$ 333.9491; found 333.9487.

2-bromo-7-iodophenanthrene-9,10-dione (11): A 25 mL 3-neck round bottom flask was charged with **10** (50 mg, 0.15 mmol) in H_2SO_4 (1.5 mL). *N*-Bromosuccinimide (29 mg, 0.16 mmol) was added, and the reaction was stirred at 25 °C for 16 h. The reaction was poured over ice (100 mL), and the precipitate was filtered to yield **11** (43 mg, 70%) as an orange solid. ^{1}H NMR (600 MHz, 25 °C, DMSO-d_6) δ = 8.31–8.21 (m, 2H), 8.18–8.03 (m, 3H), 8.00–7.89 (m, 1H) ppm. HRMS (EI) m/z: $[C_{14}H_6O_2BrI]^+$, calcd. for $[C_{14}H_6O_2BrI]$ 411.8601; found 411.8596.

2-([1,1'-binaphthalen]-2-yl)-6-bromo-11-iodo-1,4-diphenyltriphenylene (2): A 2-neck 25 mL round bottom flask was charged with **11** (83 mg, 0.20 mmol) in MeOH (2 mL). 1,3-diphenyl acetone (55 mg, 0.26 mmol) was added and the reaction mixture was heated to 75 °C. KOH (12 mg, 0.21 mmol) in MeOH (4 mL) was added drop-wise, and the reaction mixture was heated at 75 °C for 2 h. The reaction was cooled to 25 °C, and filtered. The precipitate was washed with EtOH to yield the intermediate cyclopentadienone as a green solid, which was used without further purification. A 10 mL Schlenk flask was charged with the crude cyclopentadienone (30 mg, 0.051 mmol) and **9** (16 mg, 0.056 mmol) in *o*-xylene (1 mL), and the reaction mixture was heated to 145 °C for 16 h. The reaction mixture was cooled to 25 °C and the solvent was evaporated to yield a

crude residue. Column chromatography (CH_2Cl_2/hexane 1:10) to yield **2** (20 mg, 47%) as a colorless solid. Variable temperature NMR in 1,1,2,2-tetrachloroethane-d_2 at 110 °C was performed in order to resolve NMR spectroscopic signals (Supporting Fig. S7). Even at high temperature, a fully resolved NMR was not obtained due to the high degree of rotational restriction within the molecule. Major NMR shifts at 20 °C reported as follows (Supporting Figs. S10, S11). X-ray crystallography reveals that **2** crystallizes as a 1:1 mixture of regioisomers with respect to the position of the I/Br substituent at the C6/C11 position of the triphenylene core. ^{1}H NMR (600 MHz, $CDCl_3$) δ = 8.13 (d, J = 8.7 Hz, 1H), 7.98 (d, J = 8.5 Hz, 1H), 7.91 (m, 2H), 7.85 (s, 1H), 7.80 (d, J = 8.4 Hz, 1H), 7.71–7.54 (m, 4H), 7.54–7.34 (m, 6H), 7.24–7.18 (m, 3H), 7.18–6.89 (m, 3H), 6.55–6.39 (m, 2H) ppm; ^{13}C NMR (151 MHz, 1,1,2,2-tetrachloroethane-d_2) δ = 142.9, 141.0, 139.4, 138.8, 138.2, 137.1, 136.7, 136.0, 135.7, 134.9, 133.2, 132.9, 132.7, 132.5, 132.3, 132.3, 129.3, 129.2, 128.8, 128.2, 128.0, 127.8, 127.6, 127.2, 127.2, 126.7, 126.6, 126.4, 126.0, 125.7, 125.7, 125.3, 124.9, 124.2, 124.1, 124.0 ppm. HRMS (EI) m/z: $[C_{50}H_{30}BrI]^+$, calcd. for $[C_{50}H_{30}BrI]$ 838.0563; found 838.0555.

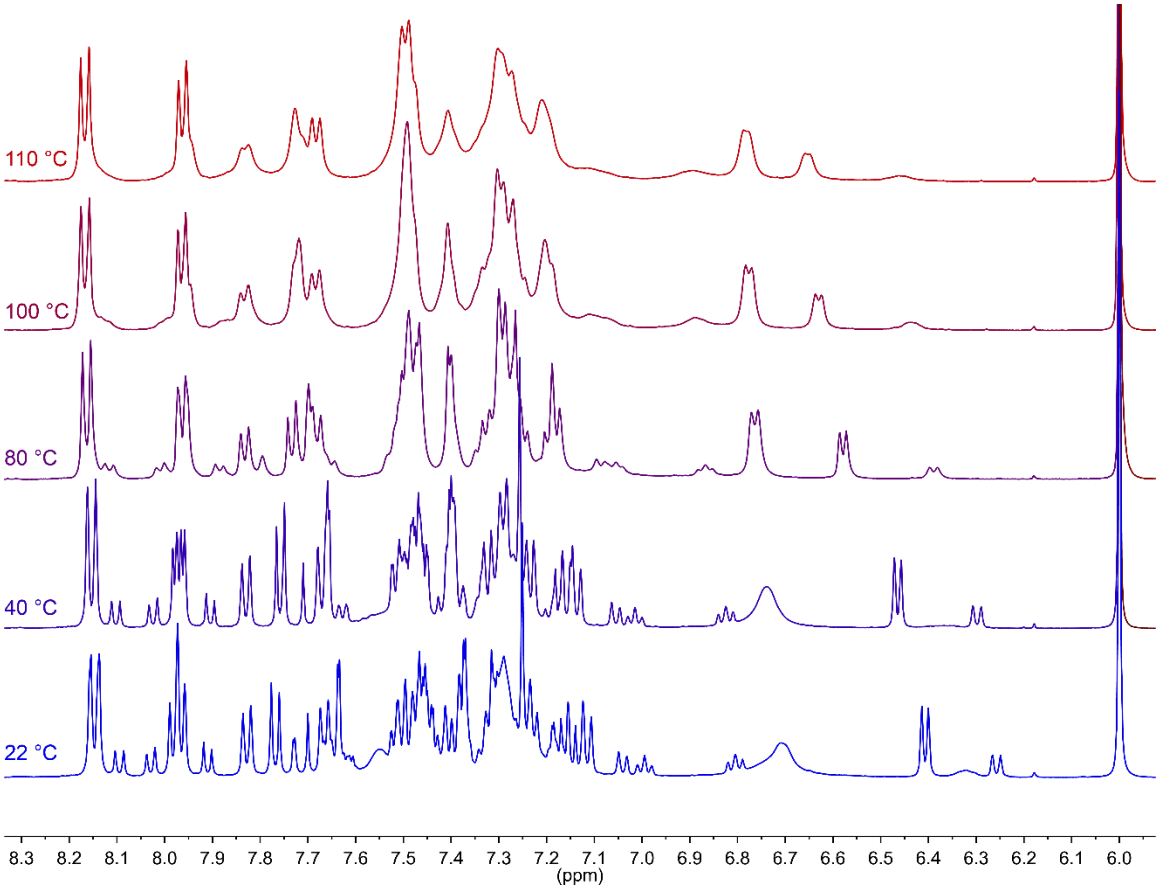

Supporting Figure S6. Variable Temperature (22–110 °C) NMR of **3**, ^{1}H NMR (500 MHz, 1,1,2,2-tetrachloroethane-d_2).

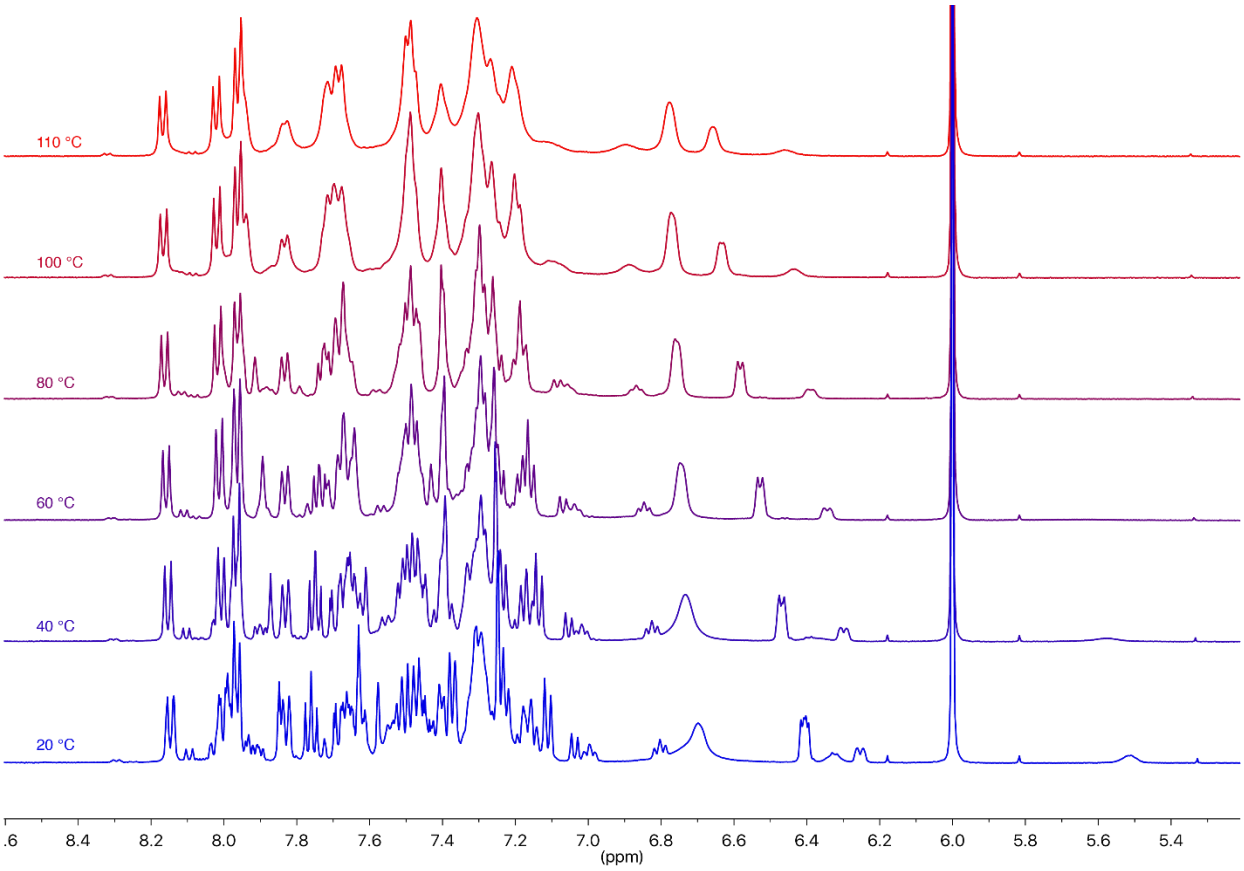

Supporting Figure S7. Variable Temperature (20–110 °C) NMR of **2**, ^{1}H NMR (500 MHz, 1,1,2,2-tetrachloroethane-d_2).

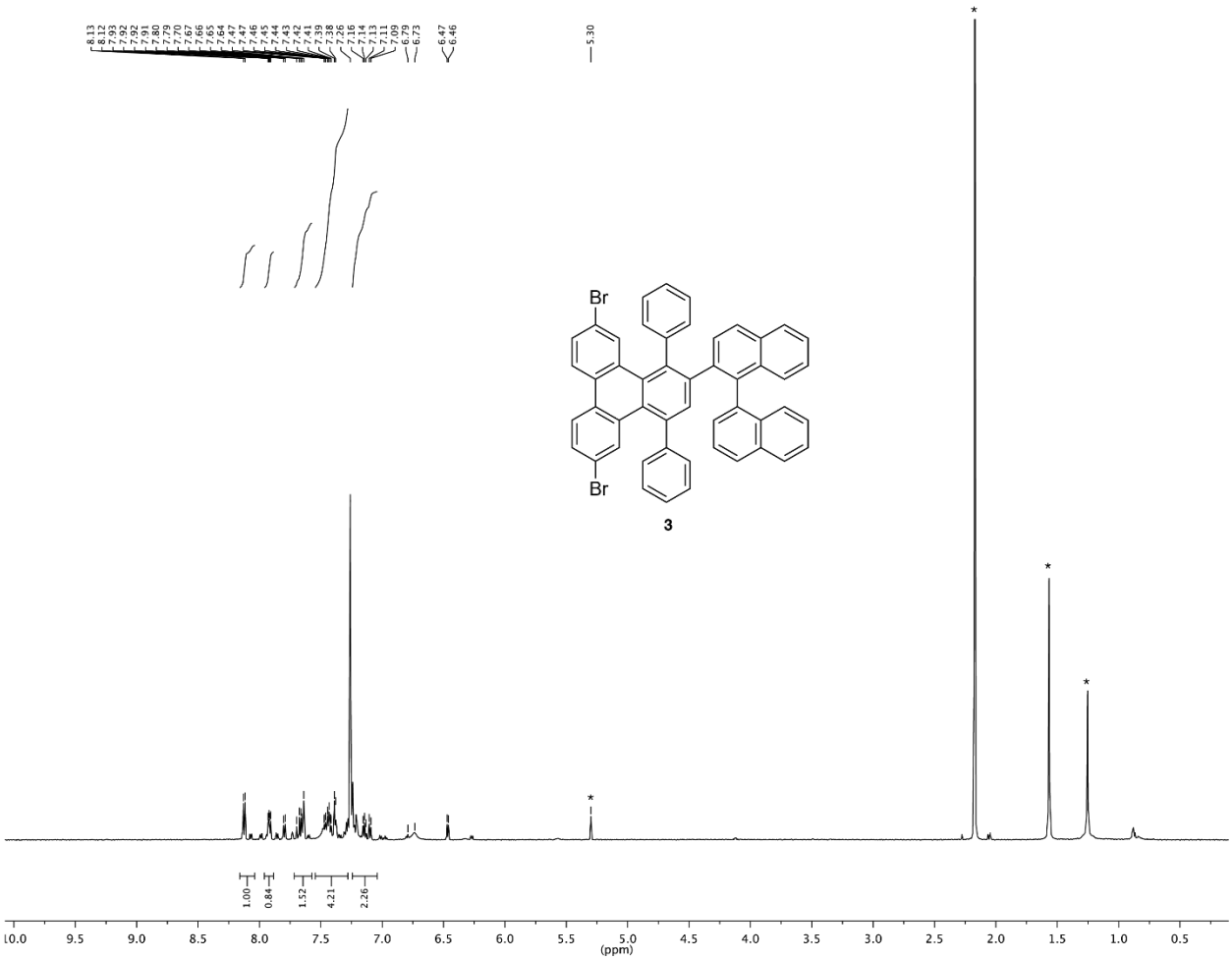

Supporting Figure S8. ^{1}H NMR (600 MHz, 20 °C, $CDCl_3$) of **3**; [*] indicate residual solvent signals.

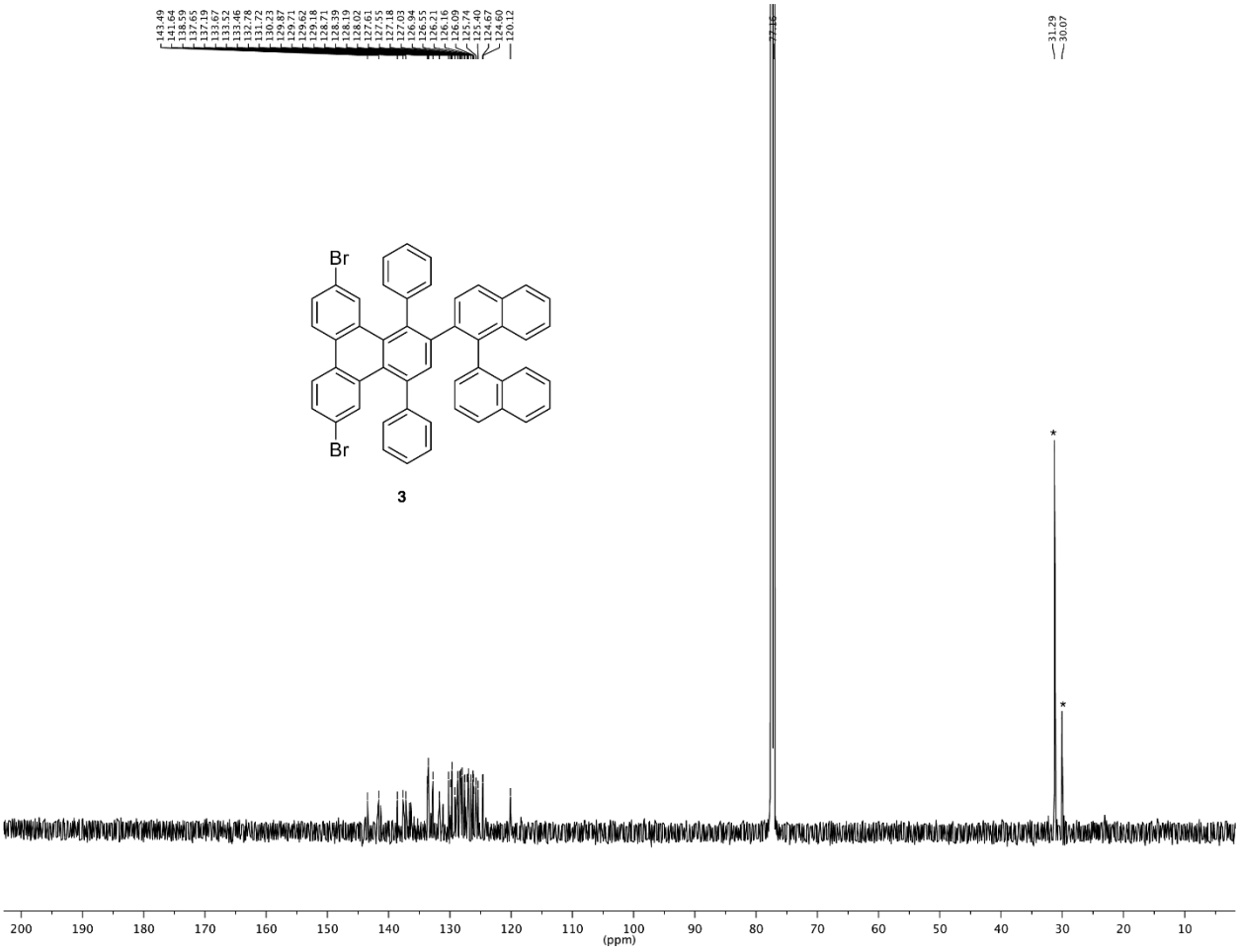

Supporting Figure S9. ^{13}C NMR (151 MHz, 20 °C, $CDCl_3$) of **3**; [*] indicate residual solvent signals.

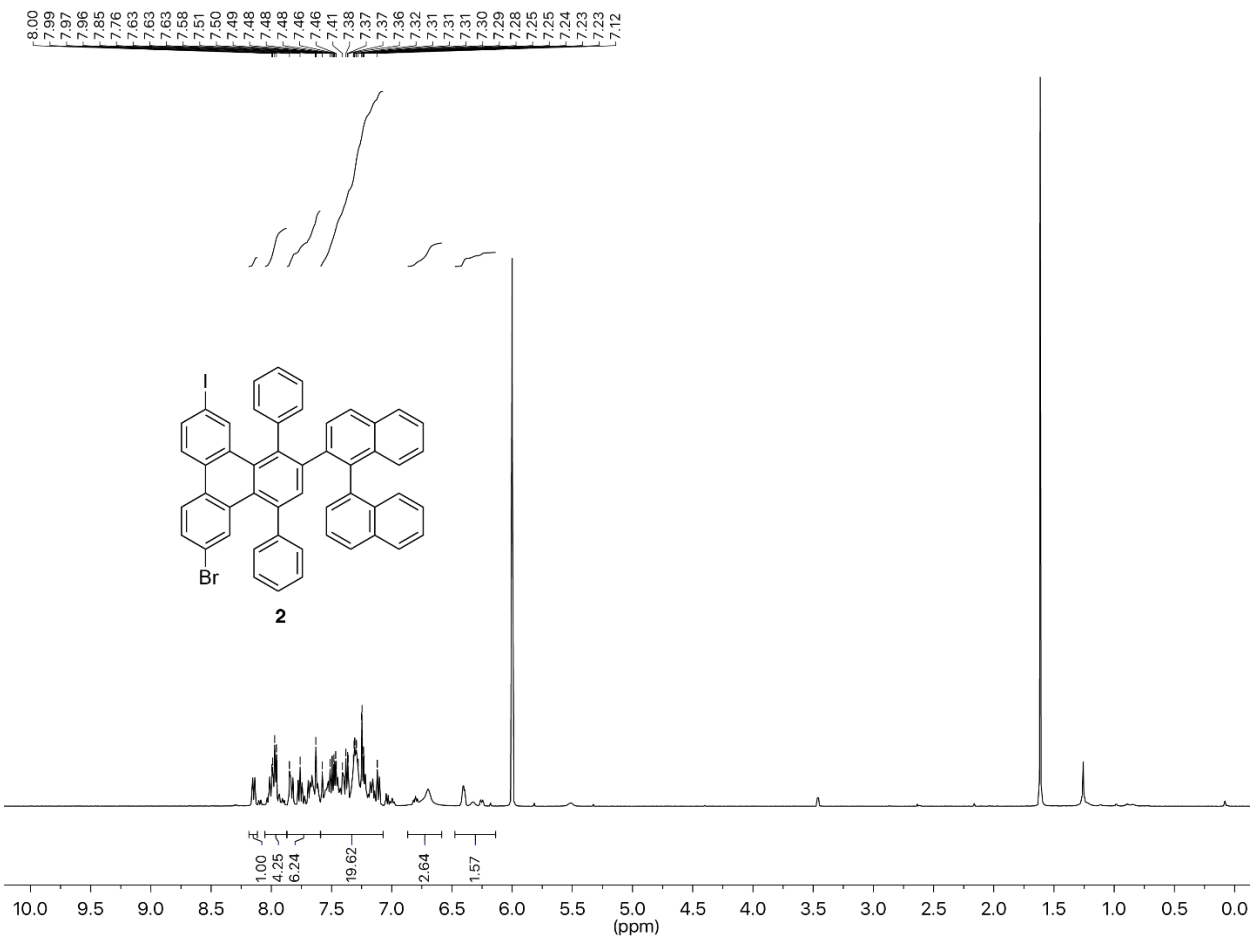

Supporting Figure S10. ^{1}H NMR (500 MHz, 20 °C, 1,1,2,2-tetrachloroethane-d_2) of **2**; [*] indicate residual solvent signals.

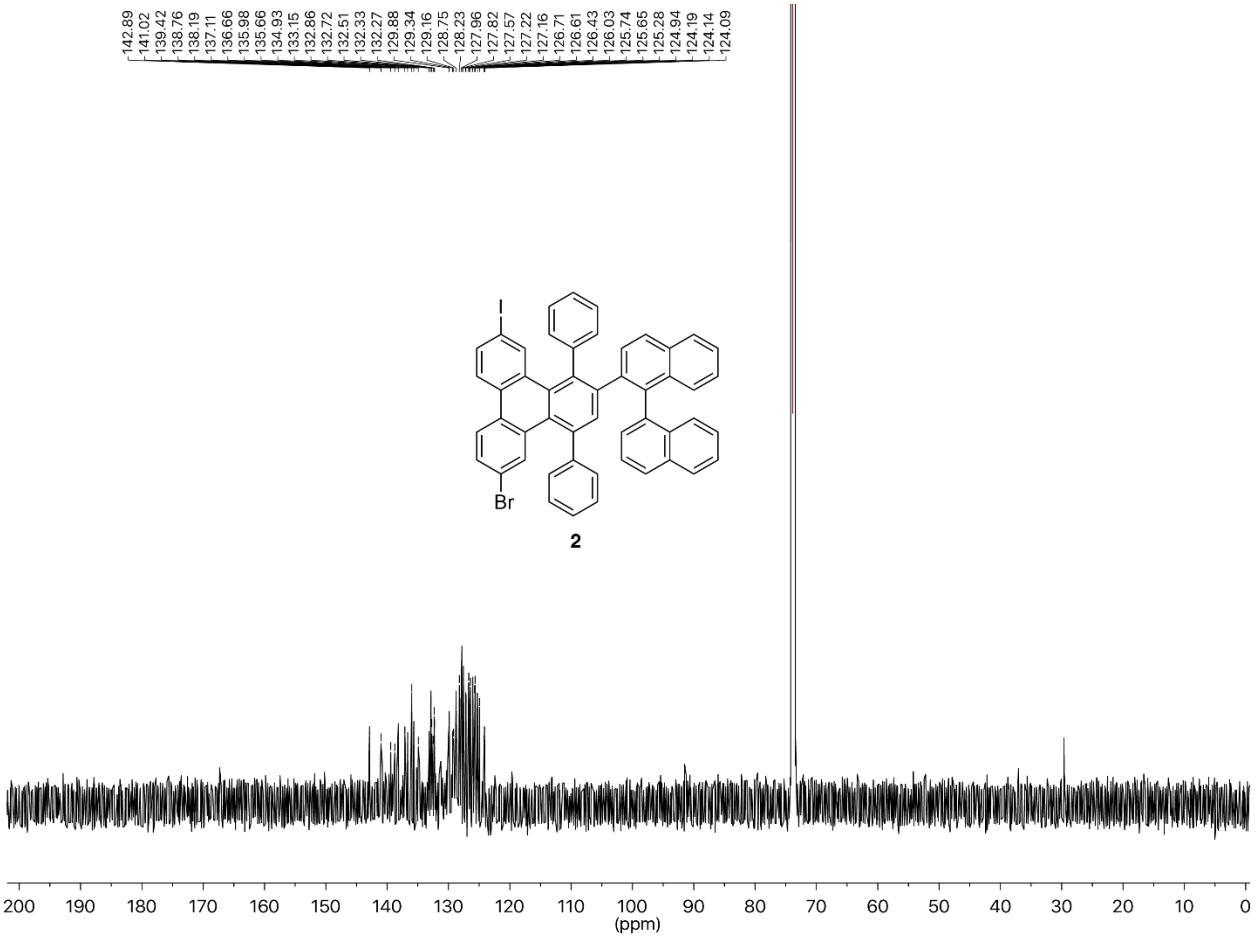

Supporting Figure S11. ^{13}C NMR (151 MHz, 20 °C, 1,1,2,2-tetrachloroethane-d_2) of **2**; [*] indicate residual solvent signals.

Supporting Table S1. Crystal data and structure refinement for **2**.

CDCC no.	1568277
Empirical formula	$C_{50}H_{30}BrI$
Formula weight	837.55
Temperature	100(2) K
Wavelength	0.71073 Å
Crystal system	Triclinic
Space group	P–1
Unit cell dimensions	a = 11.4073(4) Å α = 113.8930(10)°
	b = 12.4337(5) Å β = 91.728(2)°
	c = 13.8759(5) Å γ = 93.409(2)°
Volume	1793.07(12) $Å^3$
Z	2
Density (calculated)	1.551 Mg/m^3
Absorption coefficient	2.044 mm^{-1}
F(000)	836
Crystal size	0.070 x 0.050 x 0.050 mm^3
Theta range for data collection	1.608 to 25.457°.
Index ranges	$-13 \le h \le 13, -14 \le k \le 15, -16 \le l \le 16$
Reflections collected	97222
Independent reflections	6581 [R(int) = 0.0414]
Completeness to theta = 25.000°	99.9 %
Absorption correction	Semi-empirical from equivalents
Max. and min. transmission	0.745 and 0.643
Refinement method	Full-matrix least-squares on F^2
Data / restraints / parameters	6581 / 0 / 476
Goodness-of-fit on F^2	1.086
Final R indices [I>2sigma(I)]	R1 = 0.0254, wR2 = 0.0579
R indices (all data)	R1 = 0.0315, wR2 = 0.0622
Extinction coefficient	n/a
Largest diff. peak and hole	0.514 and –0.541 e $Å^{-3}$

Supporting Table S2. Atomic coordinates (x 10^4) and equivalent isotropic displacement parameters ($Å^2$ x 10^3) for **3**. U(eq) is defined as one third of the trace of the orthogonalized U^{ij} tensor.

	x	y	z	U(eq)
C(1)	4247(2)	5366(2)	6741(2)	15(1)
C(2)	5406(2)	5749(2)	7140(2)	16(1)
C(3)	6269(2)	4980(2)	7050(2)	15(1)
C(4)	5979(2)	3751(2)	6464(2)	15(1)
C(5)	6731(2)	2827(2)	6460(2)	16(1)
C(6)	7571(2)	3042(2)	7294(2)	19(1)
C(7)	8246(2)	2166(2)	7301(2)	23(1)
C(8)	8121(2)	1037(2)	6491(2)	26(1)
C(9)	7264(2)	798(2)	5694(2)	25(1)
C(10)	6544(2)	1668(2)	5668(2)	20(1)
C(11)	5607(2)	1408(2)	4848(2)	19(1)
C(12)	5541(2)	374(2)	3907(2)	25(1)
C(13)	4705(2)	169(2)	3104(2)	27(1)
C(14)	3930(2)	1027(2)	3220(2)	22(1)
C(15)	3949(2)	2039(2)	4130(2)	19(1)
C(16)	4767(2)	2237(2)	4977(2)	17(1)
C(17)	4876(2)	3385(2)	5888(2)	16(1)
C(18)	3958(2)	4171(2)	6133(2)	15(1)
C(19)	3399(2)	6306(2)	6976(2)	15(1)
C(20)	3041(2)	6635(2)	6151(2)	19(1)
C(21)	2343(2)	7537(2)	6331(2)	22(1)
C(22)	1980(2)	8202(2)	7348(2)	20(1)
C(23)	1253(2)	9150(2)	7558(2)	29(1)
C(24)	934(2)	9790(2)	8558(2)	32(1)
C(25)	1330(2)	9527(2)	9394(2)	29(1)
C(26)	2022(2)	8612(2)	9227(2)	22(1)
C(27)	2360(2)	7916(2)	8196(2)	17(1)

C(28)	3061(2)	6934(2)	7990(2)	16(1)
C(29)	3363(2)	6554(2)	8858(2)	16(1)
C(30)	4289(2)	7162(2)	9636(2)	17(1)
C(31)	4975(2)	8160(2)	9649(2)	21(1)
C(32)	5896(2)	8681(2)	10381(2)	26(1)
C(33)	6191(2)	8232(2)	11133(2)	29(1)
C(34)	5532(2)	7295(2)	11159(2)	27(1)
C(35)	4562(2)	6738(2)	10423(2)	21(1)
C(36)	3877(2)	5756(2)	10438(2)	23(1)
C(37)	2975(2)	5208(2)	9701(2)	22(1)
C(38)	2725(2)	5604(2)	8898(2)	18(1)
C(39)	7458(2)	5517(2)	7545(2)	17(1)
C(40)	8478(2)	5220(2)	6992(2)	20(1)
C(41)	9569(2)	5731(2)	7471(2)	26(1)
C(42)	9654(2)	6551(2)	8516(2)	31(1)
C(43)	8653(2)	6875(2)	9069(2)	26(1)
C(44)	7558(2)	6356(2)	8585(2)	20(1)
C(45)	2702(2)	3669(2)	5885(2)	17(1)
C(46)	1887(2)	3934(2)	5257(2)	24(1)
C(47)	744(2)	3408(2)	5052(2)	28(1)
C(48)	395(2)	2619(2)	5481(2)	31(1)
C(49)	1187(2)	2349(2)	6108(2)	29(1)
C(50)	2329(2)	2868(2)	6307(2)	22(1)
Br(1)	9444(8)	2520(7)	8466(5)	32(1)
I(1)	2717(4)	855(3)	2022(3)	28(1)
Br(1A)	2834(6)	720(5)	2047(5)	28(1)
I(1A)	9394(5)	2617(5)	8601(3)	32(1)

Supporting Table S3. Bond lengths [Å] and angles [°] for **2**.

C(1)-C(18)	1.391(3)
C(1)-C(2)	1.396(3)
C(1)-C(19)	1.501(3)
C(2)-C(3)	1.386(3)
C(2)-H(2)	0.9500
C(3)-C(4)	1.421(3)
C(3)-C(39)	1.492(3)
C(4)-C(17)	1.416(3)
C(4)-C(5)	1.473(3)
C(5)-C(6)	1.407(3)
C(5)-C(10)	1.413(3)
C(6)-C(7)	1.374(3)
C(6)-H(6)	0.9500
C(7)-C(8)	1.395(3)
C(7)-Br(1)	1.974(9)
C(7)-I(1A)	2.058(6)
C(8)-C(9)	1.379(3)
C(8)-H(8)	0.9500
C(9)-C(10)	1.407(3)
C(9)-H(9)	0.9500
C(10)-C(11)	1.459(3)
C(11)-C(12)	1.409(3)
C(11)-C(16)	1.411(3)
C(12)-C(13)	1.375(4)
C(12)-H(12)	0.9500
C(13)-C(14)	1.388(3)
C(13)-H(13)	0.9500
C(14)-C(15)	1.373(3)
C(14)-Br(1A)	1.918(6)
C(14)-I(1)	2.065(4)

C(15)-C(16)	1.409(3)
C(15)-H(15)	0.9500
C(16)-C(17)	1.470(3)
C(17)-C(18)	1.429(3)
C(18)-C(45)	1.500(3)
C(19)-C(28)	1.385(3)
C(19)-C(20)	1.419(3)
C(20)-C(21)	1.358(3)
C(20)-H(20)	0.9500
C(21)-C(22)	1.407(3)
C(21)-H(21)	0.9500
C(22)-C(23)	1.419(3)
C(22)-C(27)	1.423(3)
C(23)-C(24)	1.365(4)
C(23)-H(23)	0.9500
C(24)-C(25)	1.396(4)
C(24)-H(24)	0.9500
C(25)-C(26)	1.370(3)
C(25)-H(25)	0.9500
C(26)-C(27)	1.419(3)
C(26)-H(26)	0.9500
C(27)-C(28)	1.434(3)
C(28)-C(29)	1.500(3)
C(29)-C(38)	1.372(3)
C(29)-C(30)	1.424(3)
C(30)-C(31)	1.420(3)
C(30)-C(35)	1.425(3)
C(31)-C(32)	1.370(3)
C(31)-H(31)	0.9500
C(32)-C(33)	1.410(4)
C(32)-H(32)	0.9500
C(33)-C(34)	1.363(4)
C(33)-H(33)	0.9500

C(34)-C(35)	1.419(3)
C(34)-H(34)	0.9500
C(35)-C(36)	1.417(3)
C(36)-C(37)	1.362(3)
C(36)-H(36)	0.9500
C(37)-C(38)	1.416(3)
C(37)-H(37)	0.9500
C(38)-H(38)	0.9500
C(39)-C(44)	1.392(3)
C(39)-C(40)	1.397(3)
C(40)-C(41)	1.382(3)
C(40)-H(40)	0.9500
C(41)-C(42)	1.390(4)
C(41)-H(41)	0.9500
C(42)-C(43)	1.383(4)
C(42)-H(42)	0.9500
C(43)-C(44)	1.389(3)
C(43)-H(43)	0.9500
C(44)-H(44)	0.9500
C(45)-C(50)	1.397(3)
C(45)-C(46)	1.398(3)
C(46)-C(47)	1.390(3)
C(46)-H(46)	0.9500
C(47)-C(48)	1.385(4)
C(47)-H(47)	0.9500
C(48)-C(49)	1.381(4)
C(48)-H(48)	0.9500
C(49)-C(50)	1.387(3)
C(49)-H(49)	0.9500
C(50)-H(50)	0.9500

C(18)-C(1)-C(2)	119.24(19)
C(18)-C(1)-C(19)	124.44(18)
C(2)-C(1)-C(19)	116.28(18)
C(3)-C(2)-C(1)	122.92(19)
C(3)-C(2)-H(2)	118.5
C(1)-C(2)-H(2)	118.5
C(2)-C(3)-C(4)	118.40(19)
C(2)-C(3)-C(39)	116.84(18)
C(4)-C(3)-C(39)	124.71(18)
C(17)-C(4)-C(3)	118.31(18)
C(17)-C(4)-C(5)	117.64(18)
C(3)-C(4)-C(5)	123.97(19)
C(6)-C(5)-C(10)	118.32(19)
C(6)-C(5)-C(4)	121.07(19)
C(10)-C(5)-C(4)	120.33(19)
C(7)-C(6)-C(5)	120.8(2)
C(7)-C(6)-H(6)	119.6
C(5)-C(6)-H(6)	119.6
C(6)-C(7)-C(8)	121.5(2)
C(6)-C(7)-Br(1)	119.4(3)
C(8)-C(7)-Br(1)	119.1(3)
C(6)-C(7)-I(1A)	115.7(2)
C(8)-C(7)-I(1A)	122.8(2)
C(9)-C(8)-C(7)	118.3(2)
C(9)-C(8)-H(8)	120.8
C(7)-C(8)-H(8)	120.8
C(8)-C(9)-C(10)	121.8(2)
C(8)-C(9)-H(9)	119.1
C(10)-C(9)-H(9)	119.1
C(9)-C(10)-C(5)	119.1(2)
C(9)-C(10)-C(11)	121.9(2)
C(5)-C(10)-C(11)	118.98(19)
C(12)-C(11)-C(16)	118.7(2)

C(12)-C(11)-C(10)	122.0(2)
C(16)-C(11)-C(10)	119.22(19)
C(13)-C(12)-C(11)	121.9(2)
C(13)-C(12)-H(12)	119.1
C(11)-C(12)-H(12)	119.1
C(12)-C(13)-C(14)	118.6(2)
C(12)-C(13)-H(13)	120.7
C(14)-C(13)-H(13)	120.7
C(15)-C(14)-C(13)	121.5(2)
C(15)-C(14)-Br(1A)	122.0(2)
C(13)-C(14)-Br(1A)	116.5(2)
C(15)-C(14)-I(1)	116.94(19)
C(13)-C(14)-I(1)	121.54(19)
C(14)-C(15)-C(16)	120.5(2)
C(14)-C(15)-H(15)	119.7
C(16)-C(15)-H(15)	119.7
C(15)-C(16)-C(11)	118.62(19)
C(15)-C(16)-C(17)	119.76(19)
C(11)-C(16)-C(17)	120.66(19)
C(4)-C(17)-C(18)	120.02(18)
C(4)-C(17)-C(16)	117.46(18)
C(18)-C(17)-C(16)	122.20(19)
C(1)-C(18)-C(17)	118.60(19)
C(1)-C(18)-C(45)	121.54(18)
C(17)-C(18)-C(45)	119.09(18)
C(28)-C(19)-C(20)	119.67(19)
C(28)-C(19)-C(1)	121.65(18)
C(20)-C(19)-C(1)	118.35(18)
C(21)-C(20)-C(19)	121.2(2)
C(21)-C(20)-H(20)	119.4
C(19)-C(20)-H(20)	119.4
C(20)-C(21)-C(22)	121.2(2)
C(20)-C(21)-H(21)	119.4

C(22)-C(21)-H(21)	119.4
C(21)-C(22)-C(23)	122.3(2)
C(21)-C(22)-C(27)	118.70(19)
C(23)-C(22)-C(27)	119.0(2)
C(24)-C(23)-C(22)	120.7(2)
C(24)-C(23)-H(23)	119.6
C(22)-C(23)-H(23)	119.6
C(23)-C(24)-C(25)	120.3(2)
C(23)-C(24)-H(24)	119.9
C(25)-C(24)-H(24)	119.9
C(26)-C(25)-C(24)	121.0(2)
C(26)-C(25)-H(25)	119.5
C(24)-C(25)-H(25)	119.5
C(25)-C(26)-C(27)	120.4(2)
C(25)-C(26)-H(26)	119.8
C(27)-C(26)-H(26)	119.8
C(26)-C(27)-C(22)	118.55(19)
C(26)-C(27)-C(28)	121.8(2)
C(22)-C(27)-C(28)	119.61(19)
C(19)-C(28)-C(27)	119.57(19)
C(19)-C(28)-C(29)	120.51(18)
C(27)-C(28)-C(29)	119.83(18)
C(38)-C(29)-C(30)	119.8(2)
C(38)-C(29)-C(28)	118.79(19)
C(30)-C(29)-C(28)	121.36(19)
C(31)-C(30)-C(29)	122.8(2)
C(31)-C(30)-C(35)	118.3(2)
C(29)-C(30)-C(35)	118.9(2)
C(32)-C(31)-C(30)	120.9(2)
C(32)-C(31)-H(31)	119.6
C(30)-C(31)-H(31)	119.6
C(31)-C(32)-C(33)	120.7(2)
C(31)-C(32)-H(32)	119.7

C(33)-C(32)-H(32)	119.7
C(34)-C(33)-C(32)	119.9(2)
C(34)-C(33)-H(33)	120.0
C(32)-C(33)-H(33)	120.0
C(33)-C(34)-C(35)	121.1(2)
C(33)-C(34)-H(34)	119.4
C(35)-C(34)-H(34)	119.4
C(36)-C(35)-C(34)	121.6(2)
C(36)-C(35)-C(30)	119.3(2)
C(34)-C(35)-C(30)	119.0(2)
C(37)-C(36)-C(35)	120.7(2)
C(37)-C(36)-H(36)	119.7
C(35)-C(36)-H(36)	119.7
C(36)-C(37)-C(38)	120.1(2)
C(36)-C(37)-H(37)	119.9
C(38)-C(37)-H(37)	119.9
C(29)-C(38)-C(37)	121.1(2)
C(29)-C(38)-H(38)	119.5
C(37)-C(38)-H(38)	119.5
C(44)-C(39)-C(40)	118.9(2)
C(44)-C(39)-C(3)	119.16(19)
C(40)-C(39)-C(3)	121.98(19)
C(41)-C(40)-C(39)	120.8(2)
C(41)-C(40)-H(40)	119.6
C(39)-C(40)-H(40)	119.6
C(40)-C(41)-C(42)	119.6(2)
C(40)-C(41)-H(41)	120.2
C(42)-C(41)-H(41)	120.2
C(43)-C(42)-C(41)	120.4(2)
C(43)-C(42)-H(42)	119.8
C(41)-C(42)-H(42)	119.8
C(42)-C(43)-C(44)	119.8(2)
C(42)-C(43)-H(43)	120.1

C(44)-C(43)-H(43)	120.1
C(43)-C(44)-C(39)	120.6(2)
C(43)-C(44)-H(44)	119.7
C(39)-C(44)-H(44)	119.7
C(50)-C(45)-C(46)	117.9(2)
C(50)-C(45)-C(18)	117.30(19)
C(46)-C(45)-C(18)	124.83(19)
C(47)-C(46)-C(45)	120.9(2)
C(47)-C(46)-H(46)	119.5
C(45)-C(46)-H(46)	119.5
C(48)-C(47)-C(46)	120.1(2)
C(48)-C(47)-H(47)	120.0
C(46)-C(47)-H(47)	120.0
C(49)-C(48)-C(47)	119.9(2)
C(49)-C(48)-H(48)	120.1
C(47)-C(48)-H(48)	120.1
C(48)-C(49)-C(50)	120.1(2)
C(48)-C(49)-H(49)	120.0
C(50)-C(49)-H(49)	120.0
C(49)-C(50)-C(45)	121.2(2)
C(49)-C(50)-H(50)	119.4

Supporting Table S4. Anisotropic displacement parameters ($Å^2$ x 10^3) for **2**. The anisotropic displacement factor exponent takes the form: $-2p^2$ [$h^2a^{*2}U^{11}$ + ... + 2 h k a* b* U^{12}].

	U^{11}	U^{22}	U^{33}	U^{23}	U^{13}	U^{12}
C(1)	15(1)	21(1)	11(1)	9(1)	3(1)	3(1)
C(2)	19(1)	13(1)	13(1)	4(1)	-1(1)	1(1)
C(3)	14(1)	21(1)	12(1)	7(1)	2(1)	3(1)
C(4)	15(1)	18(1)	14(1)	8(1)	5(1)	4(1)
C(5)	15(1)	18(1)	20(1)	11(1)	7(1)	3(1)
C(6)	17(1)	24(1)	22(1)	14(1)	7(1)	5(1)
C(7)	17(1)	32(1)	28(1)	20(1)	6(1)	5(1)
C(8)	20(1)	25(1)	41(1)	21(1)	11(1)	9(1)
C(9)	23(1)	18(1)	33(1)	10(1)	11(1)	4(1)
C(10)	17(1)	19(1)	27(1)	12(1)	11(1)	3(1)
C(11)	17(1)	17(1)	22(1)	7(1)	8(1)	-1(1)
C(12)	22(1)	16(1)	32(1)	5(1)	10(1)	2(1)
C(13)	28(1)	18(1)	26(1)	-1(1)	9(1)	-5(1)
C(14)	24(1)	22(1)	17(1)	5(1)	2(1)	-6(1)
C(15)	20(1)	18(1)	17(1)	6(1)	5(1)	-2(1)
C(16)	16(1)	18(1)	18(1)	7(1)	6(1)	0(1)
C(17)	17(1)	17(1)	14(1)	8(1)	3(1)	1(1)
C(18)	16(1)	20(1)	12(1)	7(1)	2(1)	3(1)
C(19)	12(1)	16(1)	18(1)	7(1)	-1(1)	-1(1)
C(20)	16(1)	24(1)	18(1)	10(1)	2(1)	-1(1)
C(21)	16(1)	28(1)	29(1)	21(1)	-3(1)	-2(1)
C(22)	12(1)	17(1)	33(1)	14(1)	-2(1)	-2(1)
C(23)	22(1)	23(1)	45(2)	19(1)	-4(1)	4(1)
C(24)	22(1)	20(1)	49(2)	9(1)	-1(1)	7(1)
C(25)	20(1)	20(1)	38(1)	2(1)	2(1)	5(1)
C(26)	15(1)	18(1)	26(1)	4(1)	0(1)	1(1)
C(27)	11(1)	15(1)	25(1)	7(1)	0(1)	-1(1)

C(28)	12(1)	16(1)	19(1)	7(1)	1(1)	0(1)
C(29)	14(1)	15(1)	17(1)	4(1)	6(1)	6(1)
C(30)	17(1)	17(1)	16(1)	4(1)	6(1)	6(1)
C(31)	19(1)	20(1)	23(1)	7(1)	5(1)	4(1)
C(32)	22(1)	22(1)	27(1)	2(1)	5(1)	2(1)
C(33)	23(1)	32(1)	20(1)	-3(1)	-3(1)	5(1)
C(34)	26(1)	32(1)	17(1)	4(1)	2(1)	13(1)
C(35)	23(1)	22(1)	16(1)	7(1)	7(1)	11(1)
C(36)	26(1)	28(1)	19(1)	12(1)	7(1)	11(1)
C(37)	25(1)	22(1)	25(1)	13(1)	8(1)	5(1)
C(38)	17(1)	17(1)	19(1)	7(1)	5(1)	3(1)
C(39)	17(1)	16(1)	21(1)	11(1)	-1(1)	3(1)
C(40)	20(1)	24(1)	21(1)	14(1)	2(1)	3(1)
C(41)	16(1)	35(1)	35(1)	22(1)	3(1)	1(1)
C(42)	20(1)	32(1)	39(1)	15(1)	-7(1)	-8(1)
C(43)	25(1)	20(1)	27(1)	6(1)	-6(1)	-2(1)
C(44)	19(1)	18(1)	23(1)	8(1)	1(1)	4(1)
C(45)	17(1)	17(1)	13(1)	3(1)	2(1)	3(1)
C(46)	23(1)	25(1)	23(1)	12(1)	-2(1)	0(1)
C(47)	20(1)	35(1)	29(1)	14(1)	-5(1)	2(1)
C(48)	17(1)	41(2)	31(1)	12(1)	-2(1)	-5(1)
C(49)	22(1)	35(1)	32(1)	18(1)	3(1)	-6(1)
C(50)	20(1)	28(1)	20(1)	11(1)	0(1)	1(1)
Br(1)	32(1)	44(1)	33(1)	26(1)	7(1)	19(1)
I(1)	42(1)	25(1)	16(1)	8(1)	-8(1)	-4(1)
Br(1A)	42(1)	25(1)	16(1)	8(1)	-8(1)	-4(1)
I(1A)	32(1)	44(1)	33(1)	26(1)	7(1)	19(1)

Supporting Table S5. Anisotropic displacement parameters ($Å^2$ x 10^3) for **2**. The anisotropic displacement factor exponent takes the form: $-2p^2$ [$h^2a^{*2}U^{11}$ + ... + 2 h k a* b* U^{12}].

	x	y	z	U(eq)
H(2)	5612	6573	7488	19
H(6)	7673	3803	7859	23
H(8)	8615	446	6487	31
H(9)	7155	26	5148	30
H(12)	6090	-198	3824	30
H(13)	4659	-544	2485	32
H(15)	3406	2609	4189	23
H(20)	3294	6216	5460	23
H(21)	2096	7721	5759	26
H(23)	986	9341	6995	35
H(24)	440	10417	8686	38
H(25)	1117	9990	10089	34
H(26)	2277	8441	9804	26
H(31)	4793	8469	9144	25
H(32)	6341	9352	10381	31
H(33)	6849	8582	11620	35
H(34)	5724	7009	11680	32
H(36)	4048	5477	10967	27
H(37)	2513	4559	9726	27
H(38)	2105	5205	8379	21
H(40)	8419	4660	6278	24
H(41)	10257	5524	7089	31
H(42)	10404	6892	8852	37
H(43)	8714	7450	9777	31
H(44)	6871	6576	8966	24
H(46)	2117	4481	4966	28
H(47)	203	3591	4617	33

H(48)	-387	2264	5345	37
H(49)	948	1808	6402	35
H(50)	2866	2675	6737	27

References

[1] Chen, Y.-C.; Cao, T.; Chen, C.; Pedramrazi, Z.; Haberer, D.; de Oteyza, D. G.; Fischer, F. R.; Louie, S. G.; Crommie, M. F. Molecular Bandgap Engineering of Bottom-Up Synthesized Graphene Nanoribbon Heterojunctions. *Nat. Nanotechnol.* **2015**, *10*, 156-160.

[2] Nguyen, G. D.; Tsai, H.-Z.; Omrani, A. A.; Marangoni, T.; Wu, M.; Rizzo, D. J.; Rodgers, G. F.; Cloke, R. R.; Durr, R. A.; Sakai, Y.; Liou, F.; Aikawa, A. S.; Chelikowsky, J. R.; Louie, S. G.; Fischer, F. R.; Crommie, M. F. Atomically Precise Graphene Nanoribbon Heterojunctions from a Single Molecular Precursor. *Nat. Nanotechnol.* **2017**, *12*, 1077-1082.

[3] Satapathy, R.; Wu, Y.-H.; Lin, H.-C. Novel Thieno-Imidazole Based Probe for Colorimetric Detection of Hg^{2+} and Fluorescence Turn-on Response of Zn^{2+}. *Org. Lett.* **2012**, *14* (10), 2564–2567.

[4] Schilling, B.; Kaufmann, D. E. Suzuki Coupling of Chiral 1,1′-Binaphthyl Systems − New Synthetic Routes to Functionalize the 2- and 2,2′-Positions. *Eur. J. Org. Chem.* **1998**, *4*, 701–109.

[5] Mamane, V.; Hannen, P.; Fürstner, A. Synthesis of Phenanthrenes and Polycyclic Heteroarenes by Transition-Metal Catalyzed Cycloisomerization Reactions. *Chem. Eur. J.* **2004**, *10* (4), 4556–4575.

[6] Chaudhuri, D.; Wettach, H.; van Schooten, K. J.; Liu, S.; Sigmund, E.; Höger, S.; Lupton, J. M. Tuning the Singlet–Triplet Gap in Metal-Free Phosphorescent π-Conjugated Polymers. *Angew. Chem. Int. Ed.* **2010**, *49*, 7714–7717.